Macromolecules

pubs.acs.org/Macromolecules Article

Supramolecular Polymer Brushes: Influence of Molecular Weight and Cross-Linking on Linear Viscoelastic Behavior

Milad Golkaram, Evelyne van Ruymbeke, Giuseppe Portale, and Katja Loos*

Cite This: *Macromolecules* 2020, 53, 4810–4820 Read Online

ACCESS | Metrics & More | Article Recommendations | Supporting Information

ABSTRACT: The origin of unique rheological response in supramolecular brush polymers is investigated using different polymer chemistries (poly(methyl acrylate) (PmA) and poly(ethylene glycol) (PEG)), topologies (linear or star), and molecular weights. A recently developed hydrogen-bonding moiety (1-(6-isocyanatohexyl)-3-(7-oxo-7,8-dihydro-1,8-naphthyridin-2-yl)-urea) (ODIN) was coupled to PmAs and PEGs to form supramolecular brush polymers, the backbone of which is formed by the associated moieties. At low molecular weights of monofunctionalized polymers (both PmA and PEG), the formed brushes are mostly composed of a thick backbone (with very short arms) and are surrounded by other similar brush polymers, which prevent them from diffusing and relaxing. Therefore, the monofunctionalized PmA with a low M_n does not show terminal flow even at the highest experimentally studied temperature (or at longest time scales). By increasing the length of the chains, supramolecular brushes with longer arms are obtained. Due to their lower density of thick backbones, these last ones have more space to move and their relaxation is therefore enhanced. In this work, we show that despite similarities between covalent and transient brush polymers, the elastic response in the latter does not originate from the brush entanglements with a large M_e (entanglement molecular weight), but it rather stems from the impenetrable rigid backbone and caging effect similar to the one described for hyperstars.

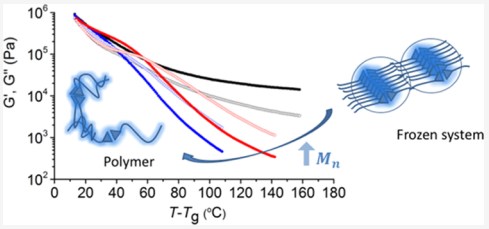

INTRODUCTION

The rheology of complex macromolecular architectures such as stars, combs, and (bottle)brushes has been investigated extensively.[1−17] In these types of polymers, important features differ from the melt dynamics of their linear analogues. For instance, it is common for brush polymers to relax sequentially and, therefore, their stress relaxation mechanism consists of the segmental regime, arm regime, and the terminal regime.[3] On the other hand, in the case of star polymers with low functionality ($f < 8$) and long arm M_a, linear dynamics are well understood and described by the model of Milner and McLeish based on arm retraction and contour length fluctuation (CLF) mechanisms;[4,18] the stress relaxes by the free end of an arm retracting inward along its primitive path and a new "tube" is formed. Since the retraction of the arm is entropically unfavorable, the arm relaxation is a slow process, which depends exponentially on the length of the arm M_a.[19,20] Therefore, the outermost segments of the arms (near the free ends) relax faster than the inner segments close to the core region of the star.[18,21] This difference between relaxation times leads to a hierarchy of length scales and relaxation time scales that characterize the dynamics of star polymers. By increasing the number of arms and/or decreasing the size of the arms, a so-called hyperstar is formed.[22−24] Hyperstars exhibit characteristics of both polymers and colloids, displaying a high-frequency relaxation of polymer segments, an intermediate-frequency plateau of entangled star arms, and then a two-step terminal relaxation characteristic of multiarm star polymers.[25] In the two-step process, a faster relaxation occurs first due to arm retraction and then a structural rearrangement of star cores, which is similar to the colloidal materials.[25] These soft colloidal particles are characterized by an inhomogeneous intramolecular monomer density containing dense and impenetrable cores, which can only relax by slow cooperative rearrangements.[24,25] In the extreme cases of more than 800 short arms, a jamming phenomenon has been reported, which prevents terminal relaxation in the accessible frequencies. Therefore, an additional plateau with low moduli values could be observed. Their low modulus makes them a good candidate for supersoft elastomers.[25] Thus, the jamming character of these hyperstars is a result of excluded volume effects, which slows down their center-of-mass motion and makes them behave as hard spheres.[25,26] Besides the star polymers, comb polymers and supramolecular comb polymers with low grafting density are also characterized by a two-step relaxation. However, this is not due to jamming but is rather attributed to the hierarchical relaxation of the branches of the comb polymer followed by the relaxation of its backbone.[27−29]

Received: January 11, 2020
Revised: May 17, 2020
Published: June 4, 2020

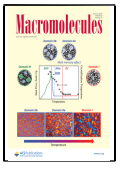

https://dx.doi.org/10.1021/acs.macromol.0c00074
Macromolecules 2020, 53, 4810–4820

Microgels can also be categorized in the same type as hyperstars since at a high grafting density, the terminal relaxation is arrested in the experimental frequency.[30] On the other hand, polymer-grafted nanoparticles (PNP) can behave similar to polymer (hyper)stars, showing viscoelastic liquid behavior (for low grafting densities and long chains) or viscoelastic solid behavior (at higher grafting densities and short chains). Although PNPs have similarities to hyperstars and microgels, they are composite materials and their core size is usually larger.[31−33] Microphase-separated block copolymers and telechelic supramolecular polymers able to create core−shell micelles can also be considered as soft colloids.[34−39] However, their dynamics is usually different from that of stable core−shell micelles; for instance, they often show higher thermorheologically complex (TRC) behavior as their phase separation depends on temperature.[40]

We have recently introduced a supramolecular system consisting of end-functionalized poly(tetrahydrofuran) (PTHF), which could mimic the melt rheological behavior of brush polymers.[41,11] A novel sticker (1-(6-Isocyanatohexyl)-3-(7-oxo-7,8-dihydro-1,8-naphthyridin-2-yl)-urea) (ODIN)[42] was used for end-group functionalization, which could undergo sextuple hydrogen bonding as well as stacking. We have shown that ODIN possesses a high propensity for aggregation and stacking. The stacking of ODIN moieties induced long-range ordering and lamellar formation with polymer and ODIN domain. Although the stacking strength is shown to be more important, the hydrogen-bonding strength is weaker than that of similar moieties such as 2-ureido-4[1*H*]-pyrimidinone (UPy).[41] Melt rheology showed that after the relaxation of the arms, in longer time scales, additional relaxation corresponding to the entire supramolecular brush polymer appears. However, due to the impossibility to access the lower frequencies (longer time scales) by melt rheology, the origin of the relaxation of the thick backbone of the polymer brush has not yet been revealed. Therefore, two possibilities were proposed, i.e., either reptation of the entire supramolecular brush polymer similar to covalent brush polymers or its relaxation through hopping mechanisms similar to hyperstars. In both scenarios, the terminal relaxation is combined with the dissociation of the supramolecular backbone at higher temperatures (or longer time scales). It has to be pointed out that the definition of the (supramolecular) brush polymer is considered to be a polymer with two or more side chains per backbone-repeating unit. We have shown that the complementary hydrogen bonding of ODIN provides us with such an architecture in a way that stacking helps (supramolecular) polymerization of the backbone and the hydrogen bonding supports the coupling of the side chains.[41] Other measurements like atomic force microscopy (AFM) can be performed to support this architecture, as small-angle X-ray scattering (SAXS) and rheology are not direct proof of such formations. In this manuscript, we describe a more accurate, yet broader view of the dynamics of these supramolecular polymers. In particular, the effect of different arm lengths in wider frequency ranges as well as chemistries and topologies is addressed to check whether the classical molecular pictures used for star and brush polymers is applicable to these novel transient analogues.

Therefore, two systems are discussed (Scheme 1):

(1) Linear poly(methyl acrylate) (PmA) (with M_n close to and higher than the critical molar mass M_c, defined as twice the molar mass between two entanglements) containing one end-functionalization by stickers, and thus able to create brushlike structures after stacking of the stickers.

(2) 1-, 2-, and 4-Arm star poly(ethylene glycol) (PEG) functionalized with stickers at the arm extremities to check the effect of cross-linking on the association of the supramolecular backbone. In this case, the cross-linking point is the middle part of the PEGs and the brush backbone forms the arrays of stacked stickers.

Scheme 1. Schematic Representation of Polymers PmA-*i*-ODIN and PEG-*j*-ODIN

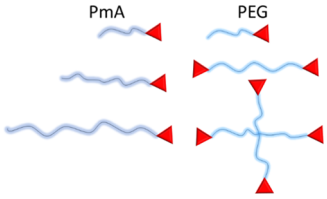

RESULTS AND DISCUSSION

Polymer Synthesis. To investigate the dynamics of supramolecular polymer brushes within a wide range of frequencies, an amorphous polymer with fairly low entanglement molecular weight was chosen so that the final polymer carries just a few entanglements. Also, the glass-transition temperature of the polymer should not be very far from the dissociation temperature of the sticker so that the interplay between sticker and chain dynamics can be observed. Considering these points, PmA is a good candidate, especially its ease of synthesis and postpolymerization modification, with reversible addition−fragmentation chain transfer (RAFT) polymerization justifying its selection. Therefore, PmAs (PmA-*i*, *i* = 6k, 18k, or 30k; see Table 1 or Scheme 2 for sample names) with three different molecular weights were obtained (Figure S1). The effect of topology and cross-linking was then tested, using commercially available star PEGs. The

Table 1. Molecular Characterization of the (Co)Polymers

entry	sample	M_n (kg mol^{-1})	$Đ$	T_g (°C)	T_c (°C)	T_m (°C)	$Z = M_n/M_e$[a] / number of arms[b]
1	PmA-6k	6	1.2	−9			∼1
2	PmA-ODIN-6k			4			
3	PmA-18k	18	1.3	−6			2
4	PmA-ODIN-18k			12			
5	PmA-30k	30	1.3	12			4
6	PmA-ODIN-30k			−12, 18			
7	PEG-1	2	1.1		38	56	1
8	PEG-1-ODIN				33	53	
9	PEG-2	4	1.1		45	59	2
10	PEG-2-ODIN				31	51	
11	PEG-4	6.7	1.1		40	57	4
12	PEG-4-ODIN				29	50	

[a]Z = number of entanglements for precursor polymer based on M_e of 7 kg mol^{-1}. [b]M_n per arm is 2 kg mol^{-1} for all samples.

https://dx.doi.org/10.1021/acs.macromol.0c00074
Macromolecules 2020, 53, 4810−4820

Scheme 2. Synthesis of Polymers PmA-*i*-ODIN and PEG-*j*-ODIN

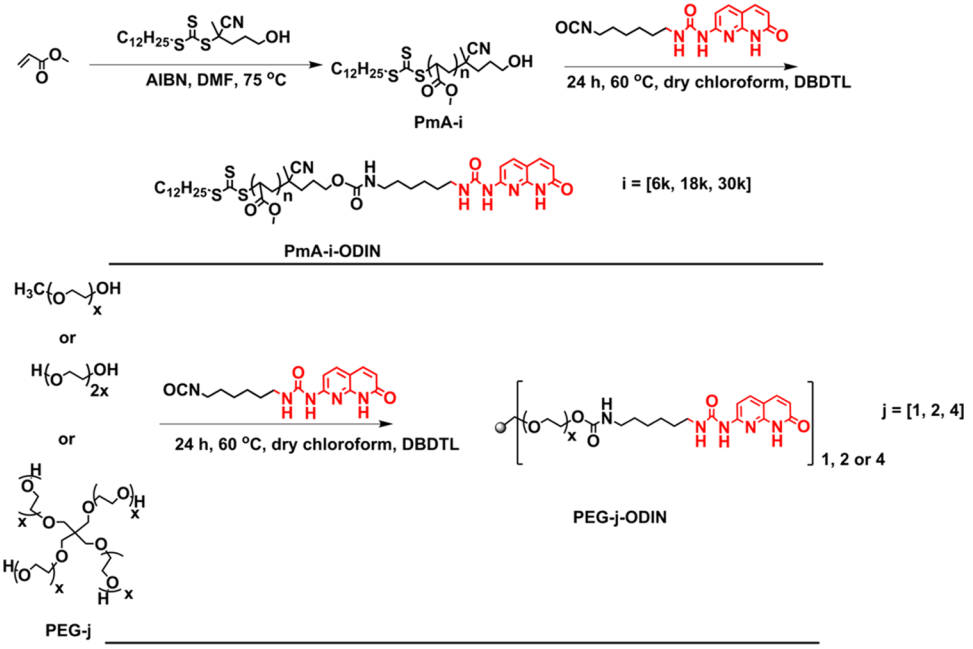

synthesis of supramolecular polymers was performed via coupling of the sticker to the hydroxyl end groups of PEG-*j* (*j* = 1, 2, or 4; Table 1 or Scheme 2). Figure 1 shows the ^{1}H NMR spectra of PmA-6k-ODIN and PEG-1-ODIN (see Figures S2 and S3 for PEG-2-ODIN and PEG-4-ODIN, respectively). The presence of ODIN protons (assigned 1−7) and the appearance of peak corresponding to urethane bond formation (assigned 8) prove the coupling of ODIN to the chain ends.

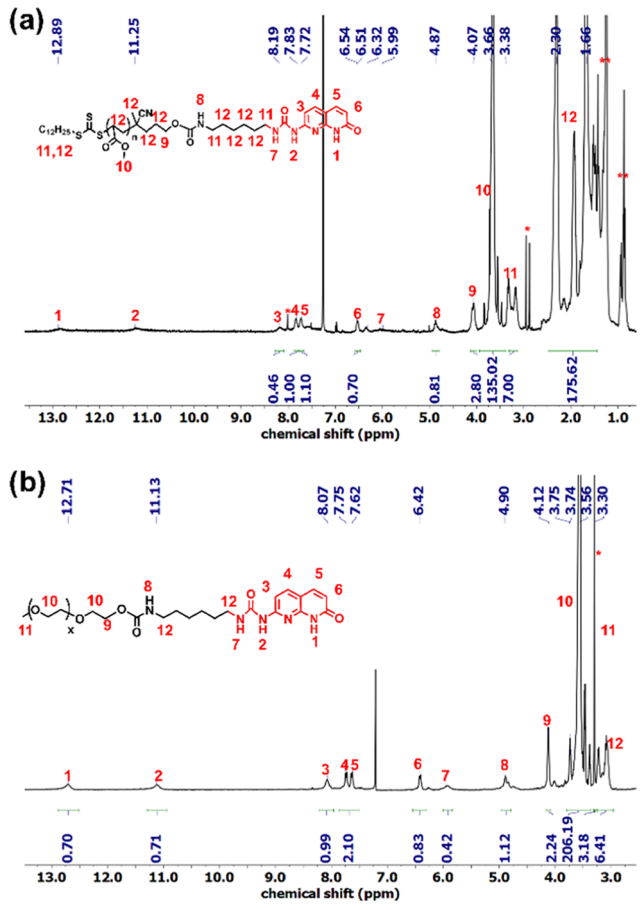

Figure 1. ^{1}H NMR spectra of PmA-6k-ODIN and PEG-1-ODIN in chloroform-*d*.

Effect of Molecular Weight: Rheology and Small-Angle X-ray Scattering (SAXS). The temperature-dependent linear viscoelastic response of PmAs shows a transition from unentangled to entangled polymer dynamics (Figure 2a). Therefore, the plateau modulus G_N of PmA can be determined from the viscoelastic data of the most entangled sample PmA-30k and is found to be equal to $G_N \simeq 0.3$ MPa (based on its frequency sweep data). Using the equation $G_N = 4/5\frac{\rho RT}{M_e}$,[43] entanglement molecular weight is calculated to be around 7 kg mol^{-1}. Figure 2b corresponds to the temperature sweep measurements (while heating) for supramolecular polymers based on PmAs. The viscoelastic response of the highest-molecular-weight polymer above M_c (red curve, PmA-30k-ODIN) displays a plateau at low temperatures (30−50 °C) with $G'_{\tan(\delta)_{min}}$ = 0.29 MPa, which is also observed with the unfunctionalized polymer ($G'_{\tan(\delta)_{min}}$ = 0.27 MPa) and is mostly due to the chain's entanglements. While the storage modulus of both PmA-18k-ODIN and PmA-30k-ODIN largely decreases at around 80 °C, their terminal relaxation is delayed (Figure 2b), compared to the unfunctionalized samples (Figure 2a). This effect is further enhanced with the lowest-molecular-weight PmA-6k-ODIN, for which a secondary plateau (with a corresponding storage modulus of around 15 kPa) is clearly observed at high temperatures. This plateau, which does not exist with the reference sample, extends until 160 °C, showing that this sample does not show viscoelastic liquid behavior within the entire studied temperature range. For PmA-6k-ODIN, the plateau modulus at lower temperatures ($G'_{\tan(\delta)_{min}}$ = 0.31 MPa) also fits well with the entanglement plateau observed for other PmA-ODINs.

https://dx.doi.org/10.1021/acs.macromol.0c00074
Macromolecules 2020, 53, 4810−4820

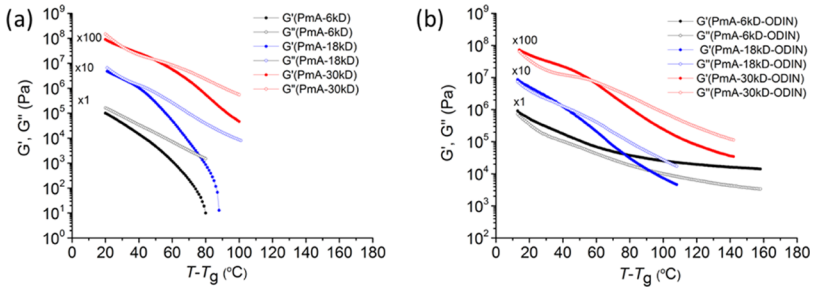

Figure 2. Temperature sweep measurements (at ω = 1 Hz) for (a) PmA-*i* and (b) PmA-*i*-ODIN using the small-amplitude oscillatory shear (SAOS) technique.

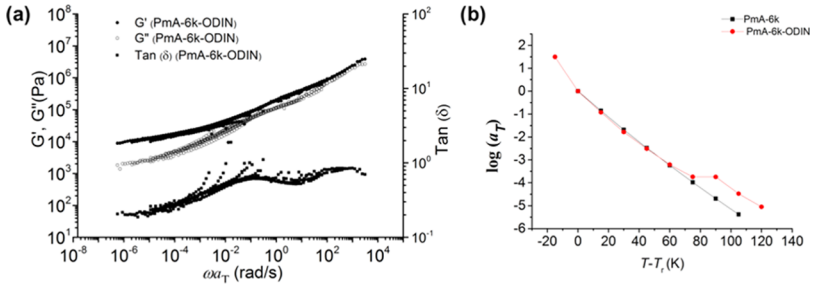

Figure 3. (a) Constructed master curve of PmA-6k-ODIN at $T \simeq T_g$ + 40 °C and (b) shift factors of PmA-6k-ODIN in comparison to PmA-6k. The shift factors were fitted using the WLF equation to access a broader temperature range.

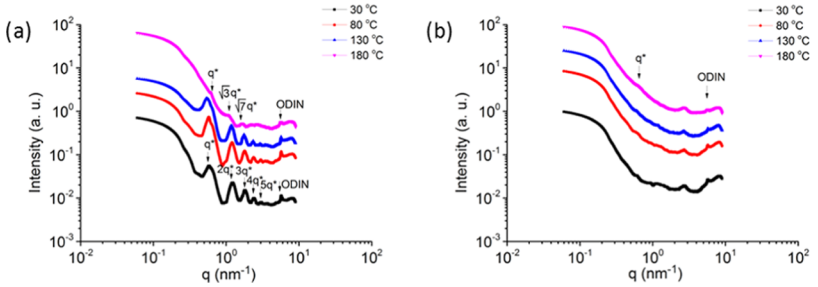

Figure 4. Variable-temperature small-angle X-ray scattering (VT-SAXS) for (a) PmA-6k-ODIN and (b) PmA-30k-ODIN at 30, 80, 130, and 180 °C (data are shifted vertically for clarity).

To have a better understanding of the origin of this plateau, frequency sweep measurements were carried out in the linear regime for the precursors (Figures S4−S6) and the supramolecular polymers (Figures S7−S9) and a master curve was constructed for PmA-6k-ODIN (Figure 3a).

A thermorheologicaly complex (TRC) behavior is observed, which is stronger in the lower-frequency side. This failure of the time−temperature superposition principle shows that the viscoelastic response has two different origins, i.e., the influence of the stickers and the chain dynamics. Two minima are found in the tan (δ) curve that are attributed to two elastic plateaus. The low-frequency plateau extends beyond the experimental frequency range. The high-frequency plateau ($G'_{\tan(\delta)_{min}}$ = 0.31 MPa) overlaps quite well with the entanglement plateau detected in Figure 2. In this high-frequency regime (lower temperature), the TRC behavior is less tangible, which is supported by comparing the shift factors of PmA-6k-ODIN and its precursor PmA-6k (Figure 3b). These ones overlap at low temperatures, meaning that the viscoelastic response is dominated by the chain's dynamics similarly to a covalent brush. In this regime, the chain-end segments localized in the center of the polymer brush are immobilized due to the stacking of their ODIN groups. Therefore, in the formed brush structure, only the side chains can relax similarly to the covalent brush polymers. It is important to note that the chain length of PmA-6k-ODIN is short in comparison to our previous study on highly entangled functionalized poly(tetrahydrofuran) (PTHF), which explains the relatively fast relaxation of the branches, compared to the slow decay of G' and G'' observed in our previous work.[41] Although the side-chain molecular weight is less than M_e, an entanglement plateau can be distinguished. This phenomenon has also been seen in covalent and supramolecular brush polymers.[44,45] This is due to the fact that each chain has one extremity that is associated, and therefore, the critical molar mass should be compared to twice the weight-average molecular weight of the chains, $2M_w$ (i.e., the molecular weight of the end-to-end molecular segments). Moreover, the dispersity of the chain length is an additional factor for this behavior.

At higher temperatures, close to but lower than the dissociation temperature of the stickers (where stacks start to lose their long-range order), shift factors diverge and show a different behavior, which manifests itself with a TRC in the low-frequency regime in Figure 3a. The secondary rubbery plateau observed at a low frequency (or a high temperature;

https://dx.doi.org/10.1021/acs.macromol.0c00074
Macromolecules 2020, 53, 4810−4820

Scheme 3. Tentative Representation of (a) PmA-6k-ODIN Colloidal Behavior and (b) PmA-18k-ODIN (or PmA-30k-ODIN) Assemblies That Lead to the Formation of Smaller Aggregates[a]

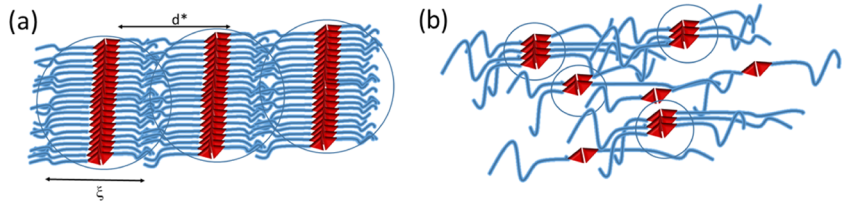

[a]The circles indicate the correlation length ξ, and d^* corresponds to the feature size of the lamellar morphology. Negligible binary associations in PmA-6k-ODIN are not shown for simplicity.

see Figure 2b) is the signature of the thick backbone of the supramolecular brushes. The fact that terminal regime is not observed means that these supramolecular backbones are unable to move and relax within the experimental frequency window. In other words, each stacked supramolecular backbone seems to be large enough to be constrained by the surrounding backbones as if it was moving in a cage formed by its neighbors. This caging effect is quite similar to the one observed with hyperstars, which act like soft colloidal particles due to their impenetrable center.[24,25] In the case of supramolecular polymer brushes, this behavior is due to the incompatibility of the ODIN and PmA, which leads to phase separation. Therefore, the penetration of PmA arms into the ODIN phase is prevented, with the core of the brushes being impenetrable. Furthermore, due to steric repulsion, the chain is most probably stretched on a scale of the correlation length ξ.[41] This would result in a thicker brush backbone since it contains both ODIN groups and the nearest arm segments up to ξ.

To investigate the influence of phase separation and the ability of the supramolecular entities to form long-range ordered morphology,[46,47] the self-assembly and morphology of the supramolecular polymers are studied at different temperatures using variable-temperature SAXS (VT-SAXS). Figure 4a shows the SAXS curve for sample PmA-6k-ODIN equilibrated at different temperatures (30, 80, 130, and 180 °C). From the position of the many scattering peaks, a long-range ordered lamellar morphology is observed up to 130 °C, while a hexagonal cylinder morphology was obtained at 180 °C. The domain spacing d^* is calculated to be 10.6 nm ($d^* = 2\pi/q^*$ with $q^* = 0.59$ nm^{-1}). Using the C−C bond length of 0.15 nm and an average degree of polymerization of 70, the polymer end-to-end distance $\langle R \rangle$ and the contour length R_{max} for an ideal chain conformation could be roughly estimated and are equal to 2.1 nm and 17.57 nm, respectively. The value of ξ is expected to be the length scale on which the chains are entirely stretched (and no penetration is allowed), and in the case of PDMS-6k-ODIN, this value is around d^*, which means that the polymer chains are partially stretched and therefore contribute to the effective backbone of the supramolecular brushes. Thus, we conclude that at each temperature for which long-range ordering is observed, PDMS-6k-ODIN are associated and stretched, and show a solidlike behavior.

By increasing the length of the chains, a larger deviation of ξ from d^* is expected, with two effects: (1) the increase in chain length leads to a lower sticker concentration, and therefore, stacking is less favorable (both due to enthalpy and entropy). (2) The polymer chains close to the sticker phase tend to phase-separate, but this effect diminishes with increasing chain length: the segments far from the sticker phase keep the ideal polymer conformation. The structure of samples PmA-ODIN-18k and PmA-ODIN-30k is therefore well represented in Scheme 3b, as supported by the short-range ordering found by VT-SAXS (Figure 4b). As discussed later, this explains why the second elastic plateau is less pronounced for these two samples.

Another possible scenario to explain the presence of a second, low-frequency plateau is considering that the supramolecular brush polymer is long enough to be entangled and show a rubbery plateau. In this case, instead of a caging effect, as described in Scheme 3, reptation of the entangled backbone should be the mechanism of stress relaxation. This way of stress relaxation is similar to covalent brush polymers with very large backbone molecular weights.[3] Using $G_N \sim M_e^{-1}$ and the apparent entanglement plateau modulus G_N^{app} of approximately 9 kPa for the diluted backbone, the entanglement molecular weight M_e for the supramolecular brush polymer backbone can be calculated to be around 2.6×10^5 g mol^{-1}. Considering that the terminal relaxation time is not visible, at least a few entanglements are expected, which means that the molecular weight should go beyond $M_n > 10^6$ g mol^{-1}, which is not reasonable. This implies that the elastic response originates from the impenetrable core of the polymer brush (colloidal behavior) rather than the brush entanglement.

Figure 5 compares the built master curves for PmA-18k and PmA-18k-ODIN. A weak entanglement plateau can be seen at

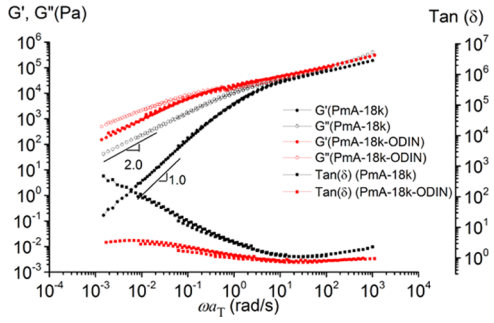

Figure 5. Built master curve of PmA-18k and PmA-18k-ODIN at $T \simeq T_g + 40$ °C using the shift factors of PmA.

the intermediate frequency from PmA-18k-ODIN with $G_N \simeq 0.3$ MPa (measured at $\tan \delta_{min}$). The presence of entanglements can be assigned to the supramolecular associations leading to double-sized polymers above M_c (Scheme 3b). At lower frequencies, a large fraction of the sample is able to relax. However, the terminal relaxation of the sample is not observed as the G' and G'' slopes do not reach values of 2 and 1, respectively, as observed with the precursor PmA-18k. Shallowing of the slopes in PmA-18k-ODIN can be attributed

https://dx.doi.org/10.1021/acs.macromol.0c00074
Macromolecules 2020, 53, 4810−4820

to the presence of aggregates in addition to binary associations of the supramolecular groups, as seen in the literature[48] (Scheme 3b).

As in Figure 5, the master curve of PmA-18k-ODIN does not show significant TRC behavior despite the fact that it is built using the shift factors of the reference sample, and it can also be concluded that the chain relaxation is dominated by the CLF and reptation process rather than by the dissociation of the stickers. This means that the lifetime of the stickers is too long to observe their dissociation, and they stay associated in the whole experimental range of frequency and temperature, with $\tau_{disentanglement} < \tau_{break}$.[49] Therefore, for PmA-18k-ODIN, a tentative scheme is drawn to include the proposed relaxation mechanism (Scheme 4): while most of the supramolecular

Scheme 4. Tentative Representation of PmA-18k-ODIN and PmA-30k-ODIN Dynamics Below the Dissociation Temperature of ODIN[a]

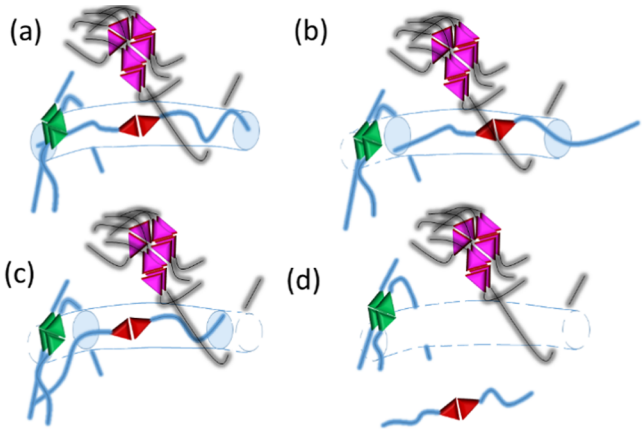

[a]The larger aggregates are shown in pink, smaller aggregates in green, and binary associations in red. The stress relaxation starts in (a) and ends in (d).

polymers relax as double linear chains (in case of binary association) or starlike molecules (in case few stickers aggregate), there are also few larger aggregates that move and relax as big objects since they are unable to dissociate. Their longer relaxation time leads to broader relaxation times and shallow terminal slopes.

As shown in Figure 5, with increasing size of the precursor polymer, the terminal relaxation time becomes longer, as expected since the reptation time of a linear polymer increases with $\tau \sim \eta \sim M^{3.4}$.[50] This is further observed in Figure 6, which shows the master curves of PmA-30k-ODIN and PmA-30k using the precursor shift factors. In this master curve, only the data obtained at low temperatures were used, to ensure thermorheological simplicity. Indeed, a significant TRC is visible in frequency sweeps performed at a higher temperature, with the association strength becoming too weak to prevent the dissociation of the ODIN groups (Figure S9). Thus, at low temperatures, one can say that the sample relaxation is dominated by the reptation and CLF processes. As for PmA-18k-ODIN, it is expected that the supramolecular association of PmA-30k-ODIN leads to the creation of double-sized chains as well as starlike molecules formed from the aggregation of few stickers (Scheme 3b). Consequently, a longer plateau is observed in comparison to the precursor polymer PmA-30k. From the G' and G'' crossover for PmA-30k-ODIN, we see

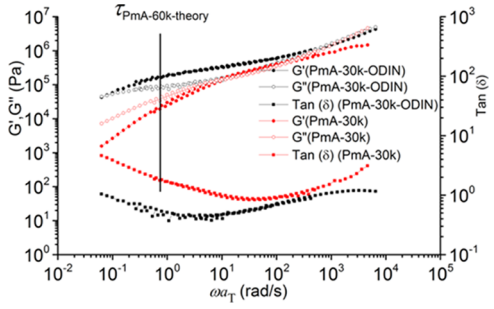

Figure 6. Master curve of PmA-30k-ODIN in comparison with PmA-30k at $T \simeq T_g + 40$ °C using the shift factors of PmA. The vertical line shows the theoretical terminal relaxation time for linear PmA with 60 kg mol^{-1} at $T = 55$ °C.

that $\tau_{disentanglement} \simeq 16$ s. Using $\tau \sim M^{3.4}$ and $\tau_{PmA-30k}$ at crossover ($T \simeq T_g + 40$ °C) (see Figure 6), the terminal relaxation time for a linear polymer with twice the molecular weight as PmA-30k should be $\tau_{60k} \simeq 1.4$ s ($\omega_{60k} \simeq 0.75$ rad s^{-1}; vertical line in Figure 6), which is shorter than that experimentally obtained ($\tau_{rel} \simeq 16$ s). However, considering starlike assemblies are present, the relaxation of the star polymers can be predicted by eq 1[6]

$$\tau_{star} \sim M_a^{3/2} \exp(M_a/M_e) \quad (1)$$

leading to relaxation times that are longer than expected by linear binary associations and are in better agreement with the experimental data. We therefore conclude that a large fraction of the stickers associates into aggregates rather than into binary association. This also explains the broad relaxation time spectrum observed in the data. It must be noted that this effect is magnified for PmA-30k-ODIN in comparison to PmA-18k-ODIN as the terminal relaxation time in star polymers scales exponentially with the arm molecular weight (eq 1). As for sample PmA-18k-ODIN, we also expect the presence of a few larger aggregates, characterized by a longer relaxation time. This is confirmed by the frequency sweeps performed at higher temperatures (Figure S9), where it is observed that the terminal regime of relaxation is not reached.

Since for this sample the dissociation of the aggregate is observed at a high temperature, the corresponding flow activation energy of the supramolecular polymer brushes can be determined, based on a similar approach to the one used by Chen et al.[51−53] as well as in our previous work.[48] Briefly, considering the relaxation of Maxwell modes, $G'(\omega) = \sum_p \omega^2\tau_p^2/(1 + \omega^2\tau_p^2)$ and $G''(\omega) = \sum_p \omega\tau_p/(1 + \omega^2\tau_p^2)$, we see that G' is more sensitive to the sticker dissociation (slow modes of relaxation) at low frequencies. Therefore, using the G' data, a master curve can be built also at high temperatures (70, 85, and 100 °C), but using different shift factors than the ones used for the reference sample. From these shift factors, an Arrhenius dependence is found, which allows us to determine the activation energy corresponding to the sticker association and was calculated to be around 99 kJ mol^{-1}. This value is similar to the activation energy found with a similar sticker (UPy), which has been reported to be 79.7 or 93.4 kJ mol^{-1}.[54]

To conclude this first part, the results show that the monofunctionalized chains associate into very stable supramolecular brushes having a thick backbone composed of both the stickers and the stretched part of the arms. While with short chains, most of the sample contributes to this backbone and the supramolecular brushes show a clear second (low

https://dx.doi.org/10.1021/acs.macromol.0c00074
Macromolecules 2020, 53, 4810−4820

frequency) elastic plateau, with increasing M_n, the sticker concentration decreases and a larger fraction of the samples can relax. Furthermore, the strength of the association is reduced, and eventually, for the higher-molar-mass chains, these last ones can dissociate at high temperatures.

Effect of Cross-Linking: Rheology and Small-Angle X-ray Scattering (SAXS). Then, we investigate the effect of cross-linking on the dynamics of supramolecular polymers. To this end, three samples, namely, PEG-1-ODIN, PEG-2-ODIN, and PEG-4-ODIN, represented in Scheme 1, were analyzed via rheology. Scheme 5a depicts the idealistic situation where

Scheme 5. Representation of PEG-4-ODIN Dynamics: (a) Idealistic Case Where the Stickers Are Stacked and (b) Realistic Picture Where Binary Associations Reduce the Mobility of the Arms, Which Prevents Them to Associate into Large Stacks[a]

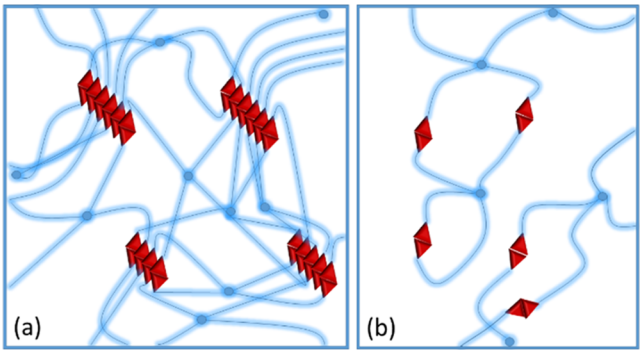

[a]The blue circles represent the cross-linking points.

stacking of the end groups can coexist with the cross-linking points. In this case, additional cross-linking should provide extra elasticity given that stacking remains intact. In this view, bifunctional PEG (PEG-2-ODIN) should also have a higher plateau modulus than PEG-1-ODIN but less than PEG-4-ODIN, as this last one is reinforced with covalent cross-linking.

Figure 7 shows the temperature sweep measurements in these samples (above T_m). For 1-arm PEG end-capped with one sticker, a plateau modulus with $G' = 5.7$ kPa is observed (Figure 7a). The level of this plateau is similar to the one observed in PmA-6k-ODIN at high temperatures ($G' = 15$ kPa) and can be attributed to the stacking of the stickers. On increasing the temperature to 60 °C, the storage modulus drops further, showing that the stacking of the stickers disappears. It must be pointed out here that both PEG-1-ODIN and PmA-6k-ODIN are short-length polymers. However, the fact that colloidal behavior persists up to the highest experimental temperature (160 °C) for PmA-6k-ODIN but only up to 60 °C for PEG-1-ODIN implies that the stacking and hydrogen bonding are significantly dependent on the chemistry of the polymer. Indeed, it has been reported that ester oxygens (−O−C═O) are much better hydrogen-bonding acceptors than ether oxygens (−O−).[55] Therefore, ODINs are more likely to make hydrogen bonding with PEG (or PTHF)[41] than with PmA or PnBa in our latest study.[56,57] This leads to an easier dissociation of the dimerized ODIN moieties in the PEG matrix in comparison to PmA, and consequently, PEG-ODINs can flow faster at higher temperatures or longer frequencies. In other words, the brush morphology is easier to be obtained in PmA.

For PEG-2-ODIN, since this polymer has two stickers at both extremities, either long linear assemblies made of several precursors (without stacking) or cross-linked supramolecular polymer brushes with the junction point being the center of PEG (similar to Scheme 5a with less cross-linking density) can be obtained. From Figure 7b, it is clear that it is this last structure that is present in this sample. Indeed, the storage modulus has significantly increased in comparison to PEG-1-ODIN ($G' = 52$ kPa), and this increase can be attributed to the formation of a network linking the supramolecular polymer brushes. However, for PEG-4-ODIN, this is not the case anymore: no elastic plateau with $G' > G''$ could be seen (see Figure 7c), even at a low temperature. The sample rather shows only slight deviations from a typical Maxwell relaxation

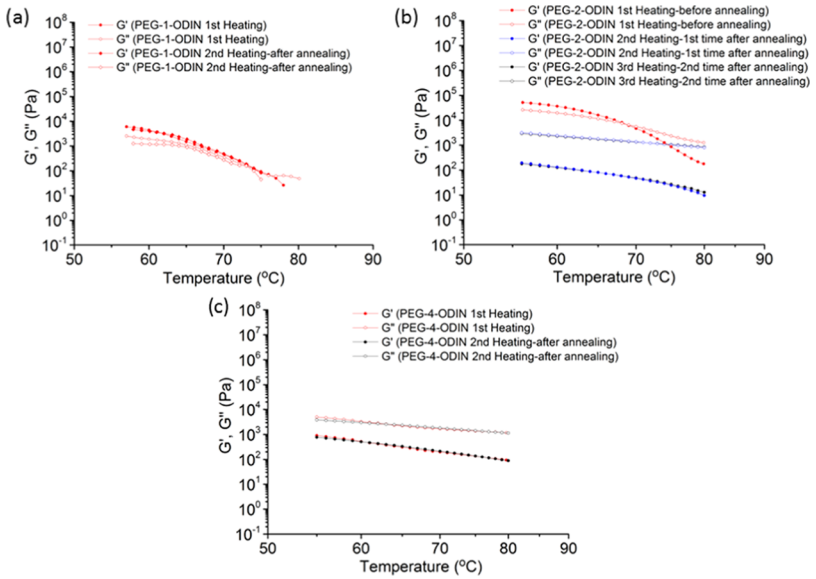

Figure 7. Temperature sweep measurements (upon heating) of (a) PEG-1-ODIN, (b) PEG-2-ODIN, and (c) PEG-4-ODIN in the linear regime above T_m. Each sample was measured before and after annealing at high temperatures. Sample PEG-2-ODIN was measured twice after annealing to check the reproducibility of the data.

https://dx.doi.org/10.1021/acs.macromol.0c00074
Macromolecules 2020, 53, 4810−4820

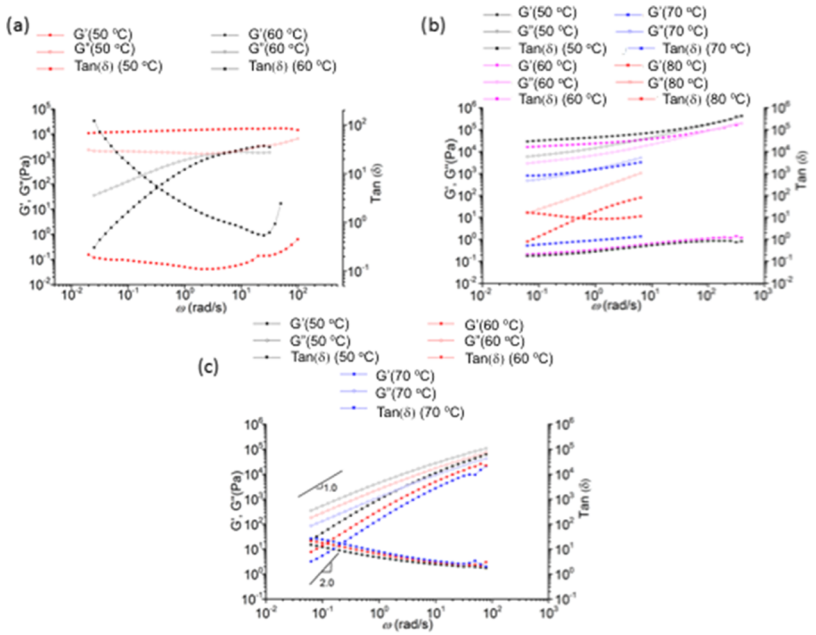

Figure 8. Frequency sweep measurements of (a) PEG-1-ODIN, (b) PEG-2-ODIN, and (c) PEG-4-ODIN in the linear regime above T_m.

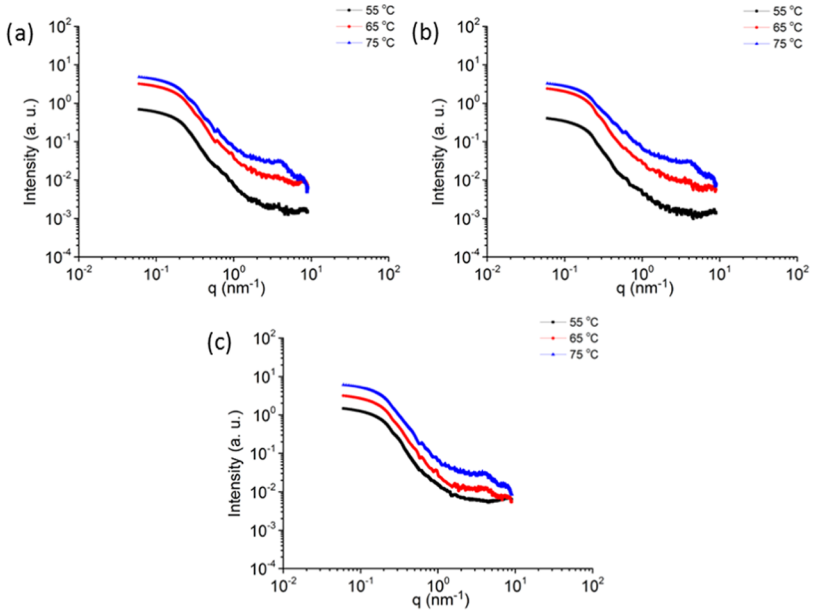

Figure 9. Variable-temperature small-angle X-ray scattering (VT-SAXS) for (a) PEG-1-ODIN, (b) PEG-2-ODIN, and (c) PEG-4-ODIN at 55, 65, and 75 °C (at $T > T_m$) (data are shifted vertically for clarity).

(Figure 8c), which suggests that no large aggregates are present in this sample. The main difference with sample PEG-2-ODIN is the fact that once binary associations occur at a short time, the system is completely frozen and the star arms cannot easily move and diffuse to allow the stickers to stack into larger aggregates. Therefore, the stickers are trapped into binary or small aggregates, which easily melt at a high temperature. Considering that a tetravalent PEG-4-ODIN needs a significant chain stretching to contribute to all stacks, the formation of the stacks is not entropically favorable. Therefore, the image in Scheme 5b is more probable. This picture can be further confirmed by annealing the samples and performing again temperature sweep measurements (Figure 7). The data for sample PEG-4-ODIN are reproducible. However, Figure 7b shows that PEG-2-ODIN has a much higher modulus when coming from low temperature, due to its ability to form larger aggregates. Directly after annealing, only binary associations have time to form and the sample behaves similar to PEG-4-ODIN.

The frequency sweeps (Figure 8) also support this hypothesis. Each sample was first heated above T_m to remove the thermal history of the polymers. Then, they were cooled down to 50 °C, to ensure that the sample crystallization does not influence the measurements ($T > T_c$). Measuring at this temperature ($T = 50$ °C) can be risky as crystallization is time-dependent, but considering that the temperature sweeps above T_m (Figure 7) show the same range of moduli, we can speculate that no crystallization occurred during the frequency

https://dx.doi.org/10.1021/acs.macromol.0c00074
Macromolecules 2020, 53, 4810−4820

sweeps. At T = 60 °C, sample PEG-1-ODIN starts to flow and terminal slopes characterized by G' and $G'' \sim \omega^2$ and ω^1 are reached (Figure 8a). This means that there is some degree of association but they cannot withstand large temperatures. It is also noteworthy that at a high temperature, with the other monofunctionalized samples PmA-18k-ODIN and PmA-30k-ODIN, the presence of aggregates was still visible despite the absence of long-range stacking (Figures 5 and 6) while in sample PEG-1-ODIN, the flow regime is reached at high temperatures (60 °C) (Figure 8a). This is probably due to the role of the PEG matrix (better hydrogen-bonding acceptor[55]) in breaking the ODIN:ODIN interactions, which reduces the probability of the ODIN groups to aggregate. On the other hand, sample PEG-2-ODIN does not flow at 60 °C (Figure 8b); however, it starts to relax at a higher temperature (80 °C), a temperature at which its terminal regime is not yet fully reached. This indicates that in PEG-2-ODIN, a larger fraction of chains can be trapped between two aggregates, preventing their relaxation. This makes sense considering that the chains are bifunctional and therefore are able to create long linear assemblies of different chain lengths, which have a larger probability to be trapped between two aggregates. As already discussed, the behavior of PEG-4-ODIN is rather different since it never shows $G' > G''$ implying that no stacking occurs in this sample, regardless of the temperature and frequency (Figure 8c).

The absence of long-range ordering is also clear from the VT-SAXS curves reported in Figure 9. The increase of temperature does not affect the ordering of the sample, and samples behave similarly to typical polymer melts. Although it could be expected that PEG-1-ODIN shows some degree of ordering around 60 °C, this is not the case here (Figure 9a). Even though PEG-1-ODIN showed some elastic behavior at around 60 °C (Figure 7a), no SAXS peak is observed. Thus, we can conclude that PEG-1-ODIN remains mostly amorphous or only small PEO crystals with very low contrast exist.

CONCLUSIONS

Using a variety of supramolecular polymers end-capped with a recently developed sticker, a wide range of dynamics could be observed depending on topology, chemistry, and molecular weight. As a rule of thumb, with low-molecular-weight samples, the high sticker concentration leads to a strong stacking of the stickers, which form supramolecular brushes with thick effective backbone unable to move and relax. With increase in the molecular weight, the sticker concentration decreases, which reduces the size and stability of the sticker aggregates. Consequently, only shallowing of the terminal slope occurs due to the distribution of relaxation times.

With PEG chains, it was observed that the association of the ODIN groups is weaker and the aggregates can dissociate at a high temperature. No stacking could be observed from SAXS measurement, and the network formation is attributed to the formation of binary H-bonding and small aggregates. It was observed that these last ones cannot form with 4-arm star precursors, due to their reduced mobility once binary H-bonds are created. This study further rules out the possibility of entanglement on the backbone of the polymer brush and supports that caging effects are responsible for the rise of an elastic plateau.

Thus, we have shown that the long-term elasticity of these polymers is due to the association of the ODIN groups and is highly dependent on (1) the nature of the polymer chains, which influence the association strength of the ODIN groups; (2) the length of the chains, which influences the proportion of stickers (which also affects their association strength) and the proportion of the polymer brush backbones that are unable to move and relax if they are too concentrated; and (3) the architecture of the precursors, unable to form large aggregates if their functionality is too high. By choosing the appropriate chemistry, functionality, and molecular weight, one can therefore control the dynamics of such samples at different time scales. The properties of these materials can be used for different applications such as supersoft elastomers and self-healing materials. On the other hand, by choosing two different polymer chemistries, a dynamic (supramolecular) brush block copolymer can be obtained, which has potential applications in photonic crystals.

ASSOCIATED CONTENT

Supporting Information

The Supporting Information is available free of charge at https://pubs.acs.org/doi/10.1021/acs.macromol.0c00074.

Experimental procedures; GPC traces; ^{1}H NMR spectra of PEG-**2**-ODIN and PEG-**4**-ODIN; and DSC curves (PDF)

AUTHOR INFORMATION

Corresponding Author

Katja Loos − *Macromolecular Chemistry and New Polymeric Materials, Zernike Institute for Advanced Materials, University of Groningen, 9747 AG Groningen, The Netherlands;* orcid.org/0000-0002-4613-1159; Phone: +31-50 363 6867; Email: k.u.loos@rug.nl

Authors

Milad Golkaram − *Macromolecular Chemistry and New Polymeric Materials, Zernike Institute for Advanced Materials, University of Groningen, 9747 AG Groningen, The Netherlands*

Evelyne van Ruymbeke − *Bio- and Soft Matter, Institute of Condensed Matter and Nanosciences, Université Catholique de Louvain, B-1348 Louvain-la-Neuve, Belgium;* orcid.org/0000-0001-7633-0194

Giuseppe Portale − *Macromolecular Chemistry and New Polymeric Materials, Zernike Institute for Advanced Materials, University of Groningen, 9747 AG Groningen, The Netherlands;* orcid.org/0000-0002-4903-3159

Complete contact information is available at: https://pubs.acs.org/10.1021/acs.macromol.0c00074

Author Contributions

The manuscript was written through contributions of all authors.

Funding

The research was supported by an NWO-VICI innovational research grant.

Notes

The authors declare no competing financial interest.

ACKNOWLEDGMENTS

The authors are grateful to Albert Woortman (RUG) for GPC measurements. E.v.R. is Research Associate of the F.S.R-F.N.R.S.

REFERENCES

(1) van Ruymbeke, E.; Bailly, C.; Keunings, R.; Vlassopoulos, D. A General Methodology to Predict the Linear Rheology of Branched Polymers. *Macromolecules* **2006**, *39*, 6248−6259.

(2) Milner, S. T.; van Ruymbeke, E.; Vlassopoulos, D.; Mierzwa, M.; Pakula, T.; Charalabidis, D.; Pitsikalis, M.; Hadjichristidis, N.; Bailly, C.; Keunings, R.; et al. Combinatorial Rheology of Branched Polymer Melts. *Macromolecules* **2001**, *31*, 865−883.

(3) Hu, M.; Xia, Y.; Mckenna, G.; Kornfield, J.; Grubbs, R. Linear Rheological Response of a Series of Densely Branched Brush Polymers. *Macromolecules* **2011**, *44*, 6935−6943.

(4) Fetters, L. J.; Kiss, A. D.; Pearson, D. S.; Quack, G. F.; Vitus, F. J. Rheological Behavior of Star-Shaped Polymers. *Macromolecules* **1993**, *26*, 647−654.

(5) Dalsin, S.; Hillmyer, M. A.; Bates, F. S. Linear Rheology of Polyolefin-Based Bottlebrush Polymers. *Macromolecules* **2015**, *48*, 4680−4691.

(6) McLeish, T. C. B.; Milner, S. T. Arm-Length Dependence of Stress Relaxation in Star Polymer Melts. *Macromolecules* **1998**, *31*, 7479−7482.

(7) Kirkwood, K.; Leal, L.; Vlassopoulos, D.; Driva, P.; Nikos, H. Stress Relaxation of Comb Polymers with Short Branches. *Macromolecules* **2009**, *42*, 9592−9608.

(8) Vlassopoulos, D.; Fytas, G.; Pakula, T.; Roovers, J. Multiarm Star Polymers Dynamics. *J. Phys.: Condens. Matter* **2001**, *13*, R855−R876.

(9) Kapnistos, M.; Vlassopoulos, D.; Roovers, J.; Leal, L. Linear Rheology of Architecturally Complex Macromolecules: Comb Polymers with Linear Backbones. *Macromolecules* **2005**, *38*, 7852−7862.

(10) Inkson, N.; Graham, R.; Mcleish, T.; Groves, D. J.; Fernyhough, C. Viscoelasticity of Monodisperse Comb Polymer Melts. *Macromolecules* **2006**, *39*, 4217−4227.

(11) Mcleish, T. Molecular Rheology of H-Polymers. *Macromolecules* **1988**, *21*, 1062−1070.

(12) Milner, S. T.; McLeish, T. C. B.; Young, R. N.; Hakiki, A.; Johnson, J. M. Dynamic Dilution, Constraint-Release, and Star−Linear Blends. *Macromolecules* **1998**, *31*, 9345−9353.

(13) Daniels, D. R.; Mcleish, T.; Crosby, B.; Young, R.; Fernyhough, C. Molecular Rheology of Comb Polymer Melts. 1. Linear Viscoelastic Response. *Macromolecules* **2001**, *34*, 7025−7033.

(14) Larson, R. G. Combinatorial Rheology of Branched Polymer Melts. *Macromolecules* **2001**, *34*, 4556−4571.

(15) van Ruymbeke, E.; Vlassopoulos, D.; Mierzwa, M.; Pakula, T.; Charalabidis, D.; Pitsikalis, M.; Hadjichristidis, N. Rheology and Structure of Entangled Telechelic Linear and Star Polyisoprene Melts. *Macromolecules* **2010**, *43*, 4401−4411.

(16) Park, S. J.; Shanbhag, S.; Larson, R. G. A Hierarchical Algorithm for Predicting the Linear Viscoelastic Properties of Polymer Melts with Long-Chain Branching. *Rheol. Acta* **2005**, *44*, 319−330.

(17) López-Barrón, C. R.; Brant, P.; Eberle, A. P. R.; Crowther, D. J. Linear Rheology and Structure of Molecular Bottlebrushes with Short Side Chains. *J. Rheol.* **2015**, *59*, 865−883.

(18) Johnson, K. J.; Glynos, E.; Sakellariou, G.; Green, P. Dynamics of Star-Shaped Polystyrene Molecules: From Arm Retraction to Cooperativity. *Macromolecules* **2016**, *49*, 5669−5676.

(19) Milner, S. T.; Mcleish, T. Parameter-Free Theory for Stress Relaxation in Star Polymer Melts. *Macromolecules* **1997**, *30*, 2159−2166.

(20) Zhu, J.; Likhtman, A.; Wang, Z. Arm Retraction Dynamics of Entangled Star Polymers: A Forward Flux Sampling Method Study. *J. Chem. Phys.* **2017**, *147*, No. 044907.

(21) Adams, C. H.; Brereton, M. G.; Hutchings, L.; Klein, P. G.; Mcleish, T.; Richards, R. W.; Ries, M. A Deuterium NMR Study of Selectively Labeled Polybutadiene Star Polymers. *Macromolecules* **2000**, *33*, 7101−7106.

(22) Roovers, J.; Zhou, L. L.; Toporowski, P. M.; van der Zwan, M.; Iatrou, H.; Hadjichristidis, N. Regular Star Polymers with 64 and 128 Arms. Models for Polymeric Micelles. *Macromolecules* **1993**, *26*, 4324−4331.

(23) Pakula, T.; Vlassopoulos, D.; Fytas, G.; Roovers, J. Structure and Dynamics of Melts of Multiarm Polymer Stars. *Macromolecules* **1998**, *31*, 8931−8940.

(24) Kapnistos, M.; Semenov, A. N.; Vlassopoulos, D.; Roovers, J. Viscoelastic Response of Hyperstar Polymers in the Linear Regime. *J. Chem. Phys.* **1999**, *111*, 1753−1759.

(25) Gury, L.; Gauthier, M.; Cloitre, M.; Vlassopoulos, D. Colloidal Jamming in Multiarm Star Polymer Melts. *Macromolecules* **2019**, *52*, 4617−4623.

(26) Vlassopoulos, D.; Cloitre, M. Tunable Rheology of Dense Soft Deformable Colloids. *Curr. Opin. Colloid Interface Sci.* **2014**, *19*, 561−574.

(27) Staropoli, M.; Raba, A.; Hövelmann, C. H.; Krutyeva, M.; Allgaier, J.; Appavou, M.-S.; Keiderling, U.; Stadler, F. J.; Pyckhout-Hintzen, W.; Wischnewski, A.; Richter, T. Hydrogen Bonding in a Reversible Comb Polymer Architecture: A Microscopic and Macroscopic Investigation. *Macromolecules* **2016**, *49*, 5692−5703.

(28) Allgaier, J.; Hövelmann, C. H.; Wei, Z.; Staropoli, M.; Pyckhout-Hintzen, W.; Lühmann, N.; Willbold, S. Synthesis and Rheological Behavior of Poly(1,2-Butylene Oxide) Based Supramolecular Architectures. *RSC Adv.* **2016**, *6*, 6093−6106.

(29) Staropoli, M.; Raba, A.; Hövelmann, C.; Appavou, M.-S.; Allgaier, J.; Kruteva, M.; Pyckhout-Hintzen, W.; Wischnewski, A.; Richter, D. Melt Dynamics of Supramolecular Comb Polymers: Viscoelastic and Dielectric Response. *J. Rheol.* **2017**, *61*, 1185−1196.

(30) Antonietti, M.; Pakula, T.; Bremser, W. Rheology of Small Spherical Polystyrene Microgels: A Direct Proof for a New Transport Mechanism in Bulk Polymers besides Reptation. *Macromolecules* **1995**, *28*, 4227−4233.

(31) Hore, M. Polymers on Nanoparticles: Structure & Dynamics. *Soft Matter* **2019**, *15*, 1120−1134.

(32) Sugimoto, M.; Ishizuka, K.; Hatano, K.; K. Sukumaran, S.; Aoki, Y. Viscoelastic Behavior of PMMA/Grafted PBA Nanoparticle Systems in the Molten State. *Rheol. Acta* **2017**, *56*, 779−785.

(33) Kim, S. A.; Mangal, R.; Archer, L. Relaxation Dynamics of Nanoparticle-Tethered Polymer Chains. *Macromolecules* **2015**, *48*, 6280−6293.

(34) Kossuth, M. B.; Morse, D. C.; Bates, F. S. Viscoelastic Behavior of Cubic Phases in Block Copolymer Melts. *J. Rheol.* **1999**, *43*, 167−196.

(35) Ruzette, A.-V.; Leibler, L. Block Copolymers in Tomorrow's Plastics. *Nat. Mater.* **2005**, *4*, 19−31.

(36) Herbst, F.; Schröter, K.; Gunkel, I.; Gröger, S.; Thurn-Albrecht, T.; Balbach, J.; Binder, W. H. Aggregation and Chain Dynamics in Supramolecular Polymers by Dynamic Rheology: Cluster Formation and Self-Aggregation. *Macromolecules* **2010**, *43*, 10006−10016.

(37) Yan, T.; Schröter, K.; Herbst, F.; Binder, W. H.; Thurn-Albrecht, T. Nanostructure and Rheology of Hydrogen-Bonding Telechelic Polymers in the Melt: From Micellar Liquids and Solids to Supramolecular Gels. *Macromolecules* **2014**, *47*, 2122−2130.

(38) Yan, T.; Schröter, K.; Herbst, F.; Binder, W. H.; Thurn-Albrecht, T. What Controls the Structure and the Linear and Nonlinear Rheological Properties of Dense, Dynamic Supramolecular Polymer Networks? *Macromolecules* **2017**, *50*, 2973−2985.

(39) Yan, T.; Schröter, K.; Herbst, F.; Binder, W. H.; Thurn-Albrecht, T. Unveiling the Molecular Mechanism of Self-Healing in a Telechelic, Supramolecular Polymer Network. *Sci. Rep.* **2016**, *6*, No. 32356.

(40) Urzhumtsev, Y. S. Time — Temperature Superposition for Thermorheologically Complex Materials. *Polym. Mech.* **1974**, *10*, 51−69.

(41) Golkaram, M.; Boetje, L.; Dong, J.; Suarez, L. E. A.; Fodor, C.; Maniar, D.; van Ruymbeke, E.; Faraji, S.; Portale, G.; Loos, K. Supramolecular Mimic for Bottlebrush Polymers in Bulk. *ACS Omega* **2019**, *4*, 16481−16492.

(42) Tellers, J.; Canossa, S.; Pinalli, R.; Soliman, M.; Vachon, J.; Dalcanale, E. Dynamic Cross-Linking of Polyethylene via Sextuple Hydrogen Bonding Array. *Macromolecules* **2018**, *51*, 7680−7691.

https://dx.doi.org/10.1021/acs.macromol.0c00074
Macromolecules 2020, 53, 4810−4820

(43) Larson, R. G.; Sridhar, T.; Leal, L. G.; McKinley, G. H.; Likhtman, A. E.; McLeish, T. C. B. Definitions of Entanglement Spacing and Time Constants in the Tube Model. *J. Rheol.* **2003**, *47*, 809−818.
(44) Callies, X.; Véchambre, C.; Fonteneau, C.; Pensec, S.; Chenal, J.-M.; Chazeau, L.; Bouteiller, L.; Ducouret, G.; Creton, C. Linear Rheology of Supramolecular Polymers Center-Functionalized with Strong Stickers. *Macromolecules* **2015**, *48*, 7320−7326.
(45) Kempf, M.; Ahirwal, D.; Cziep, M.; Wilhelm, M. Synthesis and Linear and Nonlinear Melt Rheology of Well-Defined Comb Architectures of PS and PpMS with a Low and Controlled Degree of Long-Chain Branching. *Macromolecules* **2013**, *46*, 4978−4994.
(46) Lacombe, J.; Pearson, S.; Pirolt, F.; Norsic, S.; D'Agosto, F.; Boisson, C.; Soulié-Ziakovic, C. Structural and Mechanical Properties of Supramolecular Polyethylenes. *Macromolecules* **2018**, *51*, 2630−2640.
(47) German, I.; D'Agosto, F.; Boisson, C.; Tencé-Girault, S.; Soulié-Ziakovic, C. Microphase Separation and Crystallization in H-Bonding End-Functionalized Polyethylenes. *Macromolecules* **2015**, *48*, 3257−3268.
(48) Golkaram, M.; Fodor, C.; van Ruymbeke, E.; Loos, K. Linear Viscoelasticity of Weakly Hydrogen-Bonded Polymers near and below the Sol−Gel Transition. *Macromolecules* **2018**, *51*, 4910−4916.
(49) Cates, M. E. Reptation of Living Polymers: Dynamics of Entangled Polymers in the Presence of Reversible Chain-Scission Reactions. *Macromolecules* **1987**, *20*, 2289−2296.
(50) Doi, M.; Edwards, S. F. *The Theory of Polymer Dynamics*, 1st ed.; Clarendon Press: Oxford, 1988; pp 1−391.
(51) Chen, Q.; Huang, C.; Weiss, R. A.; Colby, R. H. Viscoelasticity of Reversible Gelation for Ionomers. *Macromolecules* **2015**, *48*, 1221−1230.
(52) Zhang, Z.; Liu, C.; Cao, X.; Gao, L.; Chen, Q. Linear Viscoelastic and Dielectric Properties of Strongly Hydrogen-Bonded Polymers near the Sol−Gel Transition. *Macromolecules* **2016**, *49*, 9192−9202.
(53) Zhang, Z.; Huang, C.; Weiss, R. A.; Chen, Q. Association Energy in Strongly Associative Polymers. *J. Rheol.* **2017**, *61*, 1199−1207.
(54) Lewis, C. L.; Stewart, K.; Anthamatten, M. The Influence of Hydrogen Bonding Side-Groups on Viscoelastic Behavior of Linear and Network Polymers. *Macromolecules* **2014**, *47*, 729−740.
(55) Salim, N. V.; Hanley, T.; Guo, Q. Microphase Separation through Competitive Hydrogen Bonding in Double Crystalline Diblock Copolymer/Homopolymer Blends. *Macromolecules* **2010**, *43*, 7695−7704.
(56) Golkaram, M.; Portale, G.; Mulder, P.; Maniar, D.; Faraji, S.; Loos, K. Order−disorder transition in supramolecular polymer combs/brushes with polymeric side chains. *Polym. Chem.* **2020**, *11*, 2749−2760.
(57) Golkaram, M.; Loos, K. A Critical Approach to Polymer Dynamics in Supramolecular Polymers. *Macromolecules* **2019**, *52*, 9427−9444.

https://dx.doi.org/10.1021/acs.macromol.0c00074
Macromolecules 2020, 53, 4810−4820